Single S-tapered fiber Mach–Zehnder interferometers

Rui Yang,[1] Yong-Sen Yu,[1,3] Yang Xue,[1] Chao Chen,[1] Qi-Dai Chen,[1] and Hong-Bo Sun[1,2,4]

[1]*State Key Laboratory on Integrated Optoelectronics, College of Electronic Science and Engineering, Jilin University, 2699 Qianjin Street, Changchun 130012, China*

[2]*College of Physics, Jilin University, 119 Jiefang Road, Changchun 130023, China*

[3]*e-mail: yuys@jlu.edu.cn*

[4]*e-mail: hbsun@jlu.edu.cn*

Received September 1, 2011; revised October 5, 2011; accepted October 14, 2011; posted October 17, 2011 (Doc. ID 153862); published November 18, 2011

A fiber Mach–Zehnder interferometer (MZI) sensor, novel to our knowledge, based on a single "S"-like fiber taper has been fabricated via applying nonaxial pull in fiber tapering by a fusion splicer. The typical feature size of the structure has a length of 660 μm and the axial offset of 96 μm. This S fiber taper MZI has a refractive index (RI) sensitivity of 1590 nm/refractive index unit in the RI range of 1.409–1.425 and a strain sensitivity of about −60 pm/microstrain, which is 30 times higher than that of the normal two-taper-based MZI sensors. © 2011 Optical Society of America

OCIS codes: 060.2370, 060.2300.

Recently, optical fiber Mach–Zehnder interferometer (MZI) sensors based on tapered structures have attracted lots of interest in various physical and chemical sensing applications, such as temperature, strain, and refractive index (RI), due to their simple structure, ease of fabrication, and low cost [1–4]. The early fiber-taper-based MZI structures were fabricated by concatenating two single-mode fiber tapers [1], which were used to couple the fundamental core mode to cladding modes or reverse. When light travels the distance between the two tapers, a relative phase difference is induced between the core and cladding modes due to their different effective RIs, and light interference occurs in the output side taper. Because the cladding modes are sensitive to the surrounding refractive index (SRI), this two-taper MZI has been used for RI sensing, but the sensitivity is not satisfyingly high. Later, Wu *et al.* realized an MZI RI sensor based on three cascaded single-mode fiber tapers, in which a weak taper was sandwiched between the two tapers to enhance the sensitivity [4]. Moreover, in recent years, some novel MZI sensors were fabricated via combing fiber taper with a spot written in the fiber core by a femtosecond laser [5,6], which has been extensively used in high spatial resolution and three-dimensional controllable micromachining [7–9]. However, these kinds of fiber-taper-based MZI sensors still have a relative low sensitivity and a length of tens of millimeters, which is not compact for integrated applications. In this Letter, we propose a fiber MZI structure, novel to our knowledge, based on a single "S"-like fiber taper. The S fiber taper (SFT) is fabricated by applying nonaxial pull while stretching the fused fiber. The SFT consists of two bending sections on both sides and one taper in the middle. The fiber bending sections play the role of coupling light from core to the cladding or the reverse, and the fiber taper will enhance the measurement sensitivity. The SFT MZI sensor has a simple fabrication process, compact size (less than 1 mm), and high sensitivities for SRI and axial strain sensing.

Figure 1(a) shows the experimental setup for fabrication of the SFT. An electrical arc method was employed to fabricate the S taper on a standard telecommunication single-mode optical fiber (SMF) (SMF-28e, Corning, Inc.) using an Ericsson FSU-975 fusion splicer. A built-in fiber tapering program was chosen. The discharge current and time were set as 10 mA and 10 s, respectively. Then the fiber sample with a section (3–5 cm) of coating removed was fixed in the fiber clamps (FCs), and the segment without fiber coating was just under the discharge electrodes (DEs). The relative axial offset of the two clamps was controlled by manual operation of the fusion splicer. An axial offset of 120 μm was set by adjusting the FCs horizontally. The tilted fiber image on the LCD of the fusion splicer further confirmed the FCs were nonaxial. The transmission spectrum of the fiber was measured by an optical spectrum analyzer (OSA) (Yokogawa AQ6370B) with a supercontinuum broadband light source (BBS) (Superk Compact, NKT Photonics, Inc.). Finally, after the run button was pressed, the FCs were moving in reverse while electrodes were discharging, and the fiber was tapering by nonaxial pull. An SFT was realized by this easy nonaxial tapering process.

The optical microscope images and transmission spectrum of the SFT are shown in Fig. 2. The S-like fiber taper is clearly shown in Fig. 2(a), and the axial offset of the taper is measured to 96 μm. The angles of the two fiber bending sections are both 6.5°. Figure 2(b) shows the image after the SFT rotated 90°. The taper length is about 660 μm, and the diameter of the taper waist is about 65 μm. The transmission spectrum of this single SFT is shown in Fig. 2(c) with an insertion loss of 10 dB mainly

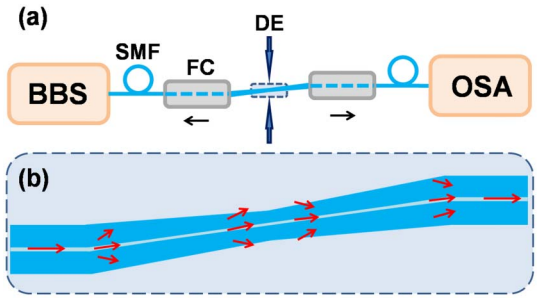

Fig. 1. (Color online) (a) Experimental setup for fabrication of the SFT. (b) Schematic diagram of the S-like fiber taper.

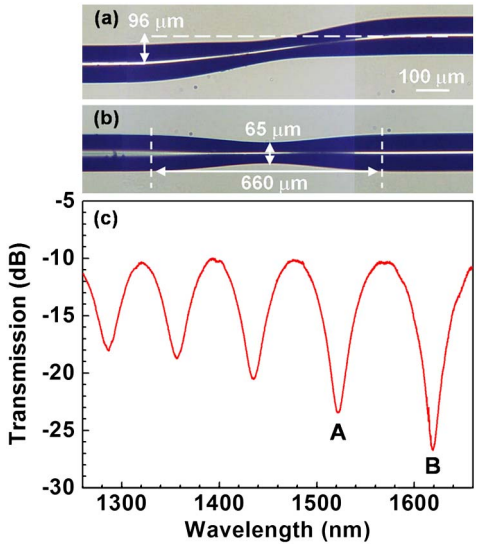

Fig. 2. (Color online) (a) Side view of the SFT in optical microscopy. (b) Top view of the SFT. (c) Transmission spectrum of the single SFT MZI in air.

due to the fiber microbending loss. Peak B has an extinction ratio (attenuation difference of maximum and minimum value) of 17 dB. The free spectral range (FSR) between peak A and peak B is about 100 nm, which is much larger than that of two- or three-taper-based MZI due to the short interference length of only about hundreds of micrometers. The FSR can be approximated by the equation in [4]. The detailed structures, such as the bending angle, the taper length, and the waist, are easily controlled by setting the relative axial offset of the two clamps in the fusion splicer, the discharge time, and the current.

A schematic diagram of light propagation in the SFT is shown in Fig. 1(b). It is not exactly the same as the cases of two- or three-taper MZI. As we know, fiber modes (core mode and cladding modes) are coupling to each other when a structure perturbation happens in the fiber, such as fiber bending. Light interference is realized in an abrupt SFT by the energy coupling from core to the cladding or reverse in the two end fiber bending parts, which have asymmetric structure and likely stimulate higher-order cladding modes [10]. The phase difference Φ between the core and cladding modes is approximated as $\Phi = 2\pi(n_{\text{eff}}^{\text{co}} - n_{\text{eff}}^{\text{cl}})L_{\text{eff}}/\lambda$, where $n_{\text{eff}}^{\text{co}}$ and $n_{\text{eff}}^{\text{cl}}$ are the effective RIs of the core and the cladding modes, respectively, L_{eff} is the effective length of the interferometer, and λ is the input wavelength. The attenuation peak wavelength λ_m of the SFT MZI can be expressed as $\lambda_m = 2(n_{\text{eff}}^{\text{co}} - n_{\text{eff}}^{\text{cl}})L_{\text{eff}}/(2m+1)$ [11], where m is the interference order. The $n_{\text{eff}}^{\text{cl}}$ is sensitive to the SRI while $n_{\text{eff}}^{\text{co}}$ is not, and both of them change with wavelength. So the difference of $n_{\text{eff}}^{\text{co}}$ and $n_{\text{eff}}^{\text{cl}}$ (Δn_{eff}) will change in two cases, which is similar to long-period fiber grating RI sensing [12]. When the order of stimulated cladding mode is relatively low, the change of Δn_{eff} is negative with the SRI increasing, and λ_m will have a blueshift, while in the case of higher-order cladding mode, the change of Δn_{eff} is positive with the SRI increasing, resulting in λ_m shifts to longer wavelength. In our experiments, the spectrum of the SFT MZI has a redshift with increments of the SRI due to the fiber bending section stimulating higher-order cladding modes.

In the measurement of the SRI, the SFT MZI sensor was fixed on a fiber holder to keep it straight with no additional stress. An adjustable stage with a microscope glass slide on its surface was placed below the SFT. The stage was then up to near the fiber, and a drop of the test RI solution was added to the SFT. The sensor was immediately immersed in the RI solution due to the small size. After the output spectrum was recorded, the SFT sensor and glass slide were cleaned with ethanol and deionized water and dried by compressed air. The procedure was repeated to measure the other RI solutions. In the experiments, the change of attenuation peak A was chosen to record, and the results of the sensor immersed in different SRIs are shown in Fig. 3. The curves in Fig. 3(a) represent cases of the SFT in different concentrations of glycerol solutions. The RIs of these glycerol solutions were collimated by an Abbe refractometer at 589 nm and room temperature (20 °C). Figure 3(a) shows that the transmission spectrum of peak A moves to longer wavelength with the SRI increasing and when the SRI reaches the effective RI of cladding mode, light interference in the SFT sensor is weakened, leading to the attenuation peaks becoming smaller and finally disappearing. The relationship between the wavelength of peak A and the SRI is shown in Fig. 3(b). A wavelength change of about 70 nm occurs with the SRI change from 1.0 to 1.425 in peak A, and the wavelength change rate becomes faster with the SRI increasing. The sensitivity of this peak in the RI range of 1.333–1.381 by linear fitting is 185 nm/refractive index unit (RIU), which is about 11 times higher than that of the normal two-taper-based MZI sensor

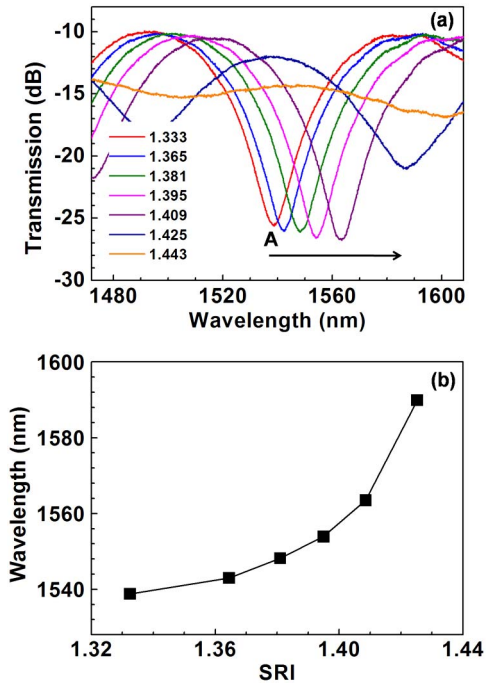

Fig. 3. (Color online) (a) Transmission spectrum of peak A changes when the SFT MZI is immersed into different RI matching solutions. (b) Relationship between the wavelength of peak A and surrounding RI.

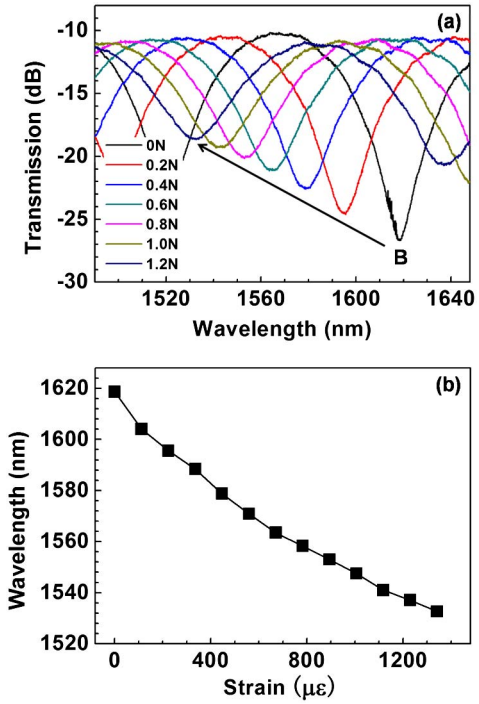

Fig. 4. (Color online) (a) Transmission spectrum of peak B changes when different axial stress is applied in the SFT MZI. (b) Relationship between the wavelength of peak B and axial strain.

and 6 times higher than that of the three-taper-based sensor. In addition, the average sensitivities of peak A in the RI range of 1.381–1.409 and 1.409–1.425 are about 554 nm/RIU and 1590 nm/RIU, respectively. The high RI sensitivity of the SFT sensor is owed to the high sensitivity to the SRI by higher-order cladding modes.

Besides RI sensing, the SFT MZI also can be used in high-sensitivity axial strain measurement. We applied axial tension to the SFT to measure its response to strain. The spectrum change of attenuation peak B under different axial tension is shown in Fig. 4(a). The transmission spectrum of the SFT shifts to a shorter wavelength, and the extinction ratio of attenuation peaks become smaller with the tension increasing. The axial tension not only elongates the SFT but also changes the effective RI of the fiber core and cladding modes. According to the formula mentioned above, the attenuation peak wavelength will have a blueshift with axial tension increasing when the influence of a decrease in the Δn_{eff} has a stronger impact than the increase of the interferometer length. Furthermore, the tension may change the shape of SFT, which loses the cladding mode energy faster, leading to the smaller attenuation peaks. The strain inside the fiber can be calculated with $\varepsilon = F/\pi r^2 E$, where F is the axial tension, r is the cladding radius, and E is the silica Young's modulus. Wavelength shifts for peak B are plotted in Fig. 4(b) as the applied strain changes. After calculation, the average strain sensitivity of peak B is about −60 pm/microstrain ($\mu\varepsilon$), which is 30 times larger than that of the two-taper MZI.

In conclusion, we have demonstrated a single S-tapered fiber MZI sensor, novel to our knowledge, for RI and axial strain measurements. The sensor used in our experiments has a length of 660 μm, and the wavelength separation of two near attenuation peaks, which are marked A and B, is about 100 nm. The transmission spectrum of the SFT has a redshift with an increasing SRI and a blueshift with increasing strain . The highest sensitivity of peak A is about 1590 nm/RIU in the RI range of 1.409–1.425, and the average axial strain sensitivity of peak B is about −60 pm/$\mu\varepsilon$. In addition to the high sensitivities to the SRI and strain, this SFT sensor has many other merits, such as simple structure, ease of fabrication, low cost, and compact size. It will find applications in chemical and physical sensing fields, especially in integrated applications.

This work was supported by the "863" and "973" programs under grants 2009AA03Z401 and 2011CB013005, respectively, and by the National Natural Science Foundation of China (NSFC) under grants 91123027, 90923037, and 60807030.

References

1. Z. Tian, S. S. H. Yam, J. Barnes, W. Bock, P. Greig, J. M. Fraser, H. P. Loock, and R. D. Oleschuk, IEEE Photon. Technol. Lett. **20**, 626 (2008).
2. Z. Tian and S. S. H. Yam, IEEE Photon. Technol. Lett. **21**, 161 (2009).
3. P. Lu, L. Men, K. Sooley, and Q. Chen, Appl. Phys. Lett. **94**, 131110 (2009).
4. D. Wu, T. Zhu, M. Deng, D. W. Duan, L. L. Shi, J. Yao, and Y. J. Rao, Appl. Opt. **50**, 1548 (2011).
5. P. Lu and Q. Chen, Opt. Lett. **36**, 268 (2011).
6. L. Men, P. Lu, and Q. Chen, IEEE Photon. Technol. Lett. **23**, 320 (2011).
7. Y. L. Zhang, Q. D. Chen, H. Xia, and H. B. Sun, Nano Today **5**, 435 (2010).
8. Y. Tian, Y. L. Zhang, J. F. Ku, Y. He, B. B. Xu, Q. D. Chen, H. Xia, and H. B. Sun, Lab Chip **10**, 2902 (2010).
9. C. Chen, Y. S. Yu, R. Yang, L. Wang, J. C. Guo, Q. D. Chen, and H. B. Sun, J. Lightwave Technol. **29**, 2126 (2011).
10. J. Thomas, N. Jovanovic, R. G. Becker, G. D. Marshall, M. J. Withford, A. Tunnermann, S. Nolte, and M. J. Steel, Opt. Express **19**, 325 (2011).
11. T. Allsop, R. Reeves, D. J. Webb, I. Bennion, and R. Neal, Rev. Sci. Instrum. **73**, 1702 (2002).
12. X. Shu, L. Zhang, and I. Bennion, J. Lightwave Technol. **20**, 255 (2002).